Magnetic domain scanning imaging using phase-sensitive THz-pulse detection ⒡

Finn-Frederik Stiewe; Tristan Winkel ⓘ ; Tobias Kleinke; Tobias Tubandt; Hauke Heyen ⓘ ; Lucas Vollroth; Ulrike Martens; Cai Müller; Jeffrey McCord ⓘ ; Jakob Walowski ✉ ⓘ ; Markus Münzenberg

CrossMark

View Online

Export Citation

Magnetic domain scanning imaging using phase-sensitive THz-pulse detection Ⓕ

View Online   Export Citation   CrossMark

Finn-Frederik Stiewe,[1] Tristan Winkel,[1] ⒾⒹ Tobias Kleinke,[1] Tobias Tubandt,[1] Hauke Heyen,[1] ⒾⒹ Lucas Vollroth,[1] Ulrike Martens,[1] Cai Müller,[2] Jeffrey McCord,[2] ⒾⒹ Jakob Walowski,[1,a] ⒾⒹ and Markus Münzenberg[1]

AFFILIATIONS

[1] Institut für Physik, Universität Greifswald, Greifswald, Germany
[2] Christian-Albrechts-Universität, Kiel, Germany

a) Author to whom correspondence should be addressed: jakob.walowski@uni-greifswald.de

ABSTRACT

In our study, we determine the alignment of magnetic domains in a CoFeB layer using THz radiation. We generate THz pulses by fs laser pulses in magnetized CoFeB/Pt heterostructures based on spin currents. An LT-GaAs Auston switch detects the radiation phase sensitively and allows us to determine the magnetization alignment. Our scanning technique with motorized stages, with step sizes in the sub-micrometer range, allows us to image two dimensional magnetic structures. Theoretically, the resolution is restricted to half of the wavelength if focusing optics in the far-field limit are used. By applying near-field imaging, the spatial resolution is enhanced to the single digit micrometer range. For this purpose, spintronic emitters in diverse geometric shapes, e.g., circles, triangles, squares, and sizes are prepared to observe the formation of magnetization patterns. The alignment of the emitted THz radiation can be influenced by applying unidirectional external magnetic fields. We demonstrate how magnetic domains with opposite alignment and different shapes divided by domain walls are created by demagnetizing the patterns using minor loops and imaged using phase sensitive THz radiation detection. For analysis, the data are compared to Kerr microscope images. The possibility of combining this method with THz range spectroscopic information of magnetic texture or antiferromagnets in direct vicinity to the spintronic emitter makes this detection method interesting for a much wider range of applications probing THz excitation in spin systems with high resolution beyond the Abbe diffraction limit, limited solely by the laser excitation area.

Magnetism has become an indispensable part of today's life. In addition to everyday applications in electrical engineering (motors and inductive charging) and medical technology (MRT), the digital storage of data in, e.g., hard disk drives or racetrack memories is also based on magnetic phenomena.[1–3] To store data, a surface is permanently magnetized, while to read out the information, the magnetic state of the respective surface is determined by a sensor.[3] Magnetic shape anisotropy also plays an important role in spin alignment.[4,5] The interaction of the magnetic energy and the exchange- and dipole–dipole interaction leads to the formation of magnetic domains. The alignment of those domains is always configured to minimize the energy in the system. Therefore, domains next to each other may have different magnetic orientations. The spatial and temporal arrangement of magnetic domains and their dynamics are the focus of the current research and in demand for new imaging methods.[6,7]

Since the first spin dynamics experiments in 1996,[8,9] many investigations into the dynamics of magnets have been carried out.[10–13] Those investigations reveal that small excitations of electrons in thin magnetic films using ultrashort laser pulses generate ultrafast spin currents.[14] Extending ferromagnetic materials (FMs) to heterostructures, in combination with non-magnetic heavy metals (NMs), these excitations can be utilized to emit radiation in the THz frequency range.[15–17] Due to the many useful properties, the demand for the development of concepts and methods utilizing this radiation for imaging is high.[16–20] The scanning technique for THz imaging in combination with near field imaging[18] has gained more attention and is used in further investigations resolving objects in

the sub-micrometer size.[21] The THz pulse phase can be controlled by the magnetization of the emitter.[17] This makes it possible to display structures depending on their magnetization direction and investigate the influence of external magnetic fields on different geometric shapes.

In this study, we use phase-sensitive detection of THz radiation to determine the magnetic state of an FM/NM heterostructure. In order to generate magnetic domains in the ferromagnetic layers of the patterned samples, the strength of the external magnetic field is systematically applied using minor loops. By using an fs laser pulse, we can generate a spatially confined THz pulse in the heterostructure and thus detect the magnetic alignment in lithographically patterned THz emitters. The micrometer sized magnetic domains require the application of near-field optics to image the changes in the magnetization direction. In Ref. 18, we presented the near-field imaging method to overcome the Abbe limit stating that spatial resolution is limited by half of the involved wavelength, which is larger than 100 μm for radiation at 1 THz frequency. We investigate spintronic THz emitters, which can be placed in direct proximity to the detector. The strong focusing of the used laser pulses down to the micrometer range confines the spatial expansion of the generated THz source spot to the dimensions of a few

micrometers. The test structure consists of many spintronic emitters with different geometric shapes and sizes (from 10 to 100 μm), which were lithographically fabricated on a glass substrate. The 2D-scanning technique with motorized stages makes it possible to record a temporal THz spectrum at each position of the sample and thus image the patterns. Despite a smaller achievable spatial resolution than magneto optical effects such as the Kerr or Faraday effect, this approach does not rely on large magneto optical response and has the capability of small field change detection in the μT range.[22]

The optical setup for detection and imaging magnetic domains is shown schematically in Fig. 1(a). The operation principle is explained in detail in Ref. 18. For THz-radiation generation, a Ti:Sa laser (Coherent Vitara, 40 fs pulse duration, 810 nm central wavelength, and 80 MHz repetition rate) is used. A beam splitter divides the laser into a lower-powered probe (dashed line) and a higher-powered pump beam (solid line). The probe beam is guided to an Auston switch (photoconductive antenna, PCA) through a delay stage. This PCA acts as a THz detector. The laser pulse short-circuits the antenna by exciting electrons in the PCA gap. The pump beam is guided to the THz emitter sample. A polarizer in the beam path enables laser power adjustment. A chopper modulates the pump beam with a frequency of 1.5 kHz. The beam is focused onto the
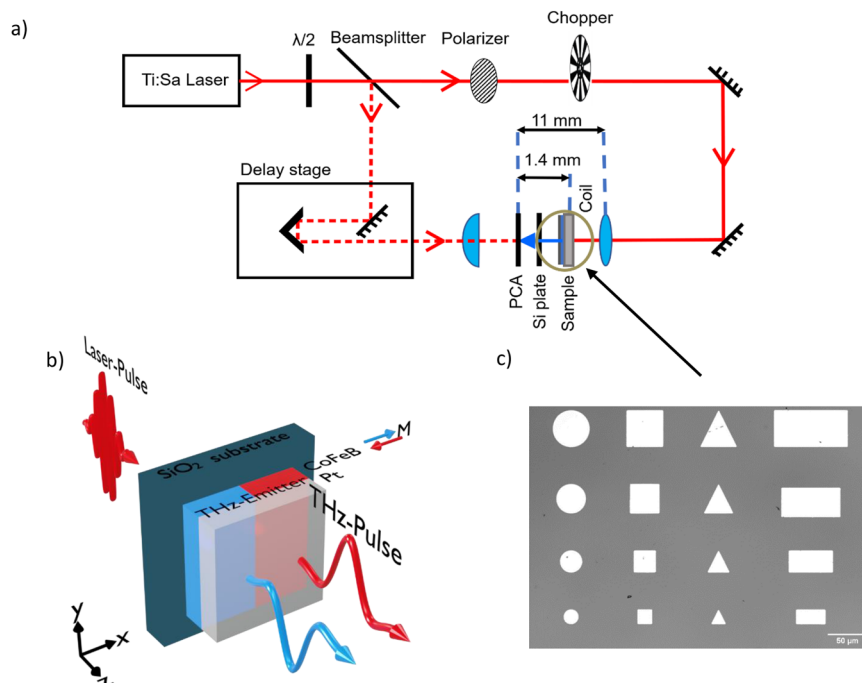

FIG. 1. (a) Setup: the light source is a Ti:sapphire laser system (central wavelength 810 nm, repetition rate 80 MHz, and pulse duration 40 fs). Behind a beam splitter, the probe beam is guided to a delay stage to adjust the temporal arrival at the photoconductive antenna detector (PCA) for signal sampling. The pump beam is directed to the spintronic emitter (sample). A polarizer allows laser power adjustment. The signal is recorded via a lock-in amplifier and modulated by a chopper. (b) Schematic of a THz-emitter heterostructure. A femtosecond laser pulse excites the ferromagnetic layer (FM) and generates a spin current. Through the inverse spin Hall effect (ISHE), the current is converted into a transient charge current in the non-magnetic layer (NM). The emitted THz has a different phase depending on the magnetization, shown in blue and red. (c) Microscopic image showing the investigated geometrical structures on the sample (light gray). They act as spintronic emitters, have the same time as magnetic structures, and have sizes ranging from 100 μm down to 10 μm.

sample, which emits THz radiation generated in the CoFeB/Pt het-erostructures (details given in Refs. 14, 18, 23, and 24). Helmholtz coils are placed around the sample to control the magnetization state by applying magnetic fields up to 4 mT and continuously reducing the field strength. This sample demagnetization using minor loops generates magnetic domains. They are imaged by scanning the sample with two motorized μm-stages moving the heterostructure horizontally and vertically (x- and y-directions) against the pump-beam with minimal step sizes of 200 nm. The emitted THz pulses are sampled by delaying the probe beam time, and the amplified signal is recorded by a lock-in amplifier.

The data are analyzed using the following procedure. A com-plex value z consisting of x + yi from the data is recorded by the lock-in amplifier. In the first step, we calculate the phase of the real signal in the complex z values. This is done by transforming the z val-ues into polar coordinates, performing a discrete Fourier transform, and picking the phase of the value representing the second har-monic. The original z values are rotated by subtracting the obtained phase, setting the imaginary part to 0 and leaving only the real part of z for further calculation. In the second step, the signal is transformed using fast Fourier transform (FFT) to obtain the frequency spectra in the THz signals. The resulting THz frequency spectra have again a real and a complex component. By determining the phase and rotat-ing it, the signal shifted to the real component. In general, we use the 1 THz amplitude from each recorded THz spectrum combined into one image to represent the magnetization state.

The investigated sample is schematically shown in Fig. 1(b). Figure 1(c) shows a microscopic image of the spintronic emitters (bright forms) patterned into different shapes and sizes from a film, deposited on a glass substrate. To create a spintronic emitter, a 2 nm thick CoFeB layer is magnetron-sputtered onto the substrate, directly followed by a 2 nm Pt layer deposited by e-beam evaporation without breaking the vacuum conditions. After thin film deposi-tion, the layer stack is coated with a negative resist (AR-N4340) and subsequently baked on a hot plate. The resist was exposed using a laboratory mask aligner (MJB4, Süss MicroTec) with a wavelength of 405 nm. Afterward, the unexposed resist is removed by develop-ment with AR 300-47. The uncovered, resist-free areas are Ar-etched in a home-built system. This leaves spintronic emitters with various geometrical shapes on the glass substrate, as shown in Fig. 1(c).

Figure 2 depicts two-dimensional THz images of the test pat-tern [Fig. 1(c)] for two extracted frequencies f = 1.0 THz and f = 1.5 THz. The images are obtained by scanning a sample area of

$420 \times 310 \ \mu m^2$ in x- and y-directions, with a step size of $s_{xy} = 2 \ \mu m$. The white area in the lower left corner originates from rotation of the image. During the measurement, the sample was slightly canted by 5° and rotated afterward for better visibility. A few data points are missing in the lower left corner indicated by the white area.

At each position, a temporal spectrum of the THz pulse is recorded. By using fast Fourier transformation (FFT), the included frequencies are extracted from each spectrum, as described above. We show normalized THz e-field amplitudes A for the frequencies f = 1.0 THz [Fig. 2(a)] and f = 1.5 THz [Fig. 2(b)]. The geometri-cal structures are clearly imaged in red color and indicated by black edges for better visibility. The environment around these structures, where the CoFeB/Pt layer is removed, only shows a small amplitude within the noise level (light red). In general, the larger shapes show a larger A than the smaller ones. This is a result of the small struc-ture size compared to the scanning laser beam. For both frequencies, the circular structures exhibit a slightly larger THz signal amplitude than the other geometrical shapes because the shape anisotropy is not direction-dependent and the sample was lightly canted during measurement while applying only a small field of 4 mT.

Figure 3 shows an overview scan of a $450 \times 350 \ \mu m^2$ area obtained with a step size of $s_{xy} = 10 \ \mu m$. The magnetic structures are imaged after demagnetization using minor loops to create magnetic domains for two distinct frequencies f = 1.0 THz and f = 1.5 THz. The Helmholtz coils are placed around the sample, as indicated in the schematic in Fig. 1(a), to align the applied field direction along the y-position axis (Figs. 2 and 3) and in the plane of the magnetic sample.

Our phase sensitive detection method shows the formation of domains with opposite magnetization in several geometrical struc-tures in Figs. 3(a) and 3(b). The overview scan was carried out in two parts. The data points around the y-position 150 μm are missing because the second part was started at a lower position, leaving out the blank area without magnetic structures.

Creating magnetic domains in the structures is very sensitive to the applied field resolution and settings. Obtaining a resolution around 0.1 mT is not sufficient to reliably create identic mag-netic domains after each procedure. Some structural magnetizations switched entirely, applying those field steps in one or the other direc-tion. This shows the apparent random magnetization orientation for the involved structures. By applying a positive magnetic field, all pat-terns show positive THz e-field amplitudes (see Fig. 2). Reversing the magnetic field flips the spins and switches to a negative THz E-field
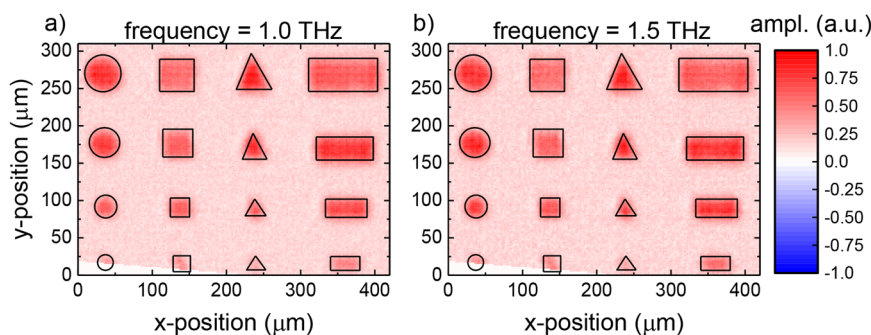

FIG. 2. Two-dimensional THz images of the magnetized sample on an $450 \times 300 \ \mu m^2$ area scanned with a step size of $s_{xy} = 2 \ \mu m$ extracted for the frequen-cies (a) f = 1.0 THz and (b) f = 1.5 THz. The THz emitting structures can be seen clearly for all included sizes. The images are rotated by 4.8° to align the structures for better visibility.
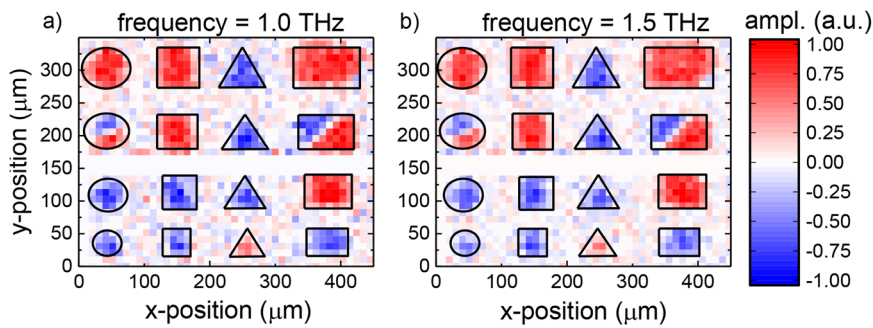
FIG. 3. Two-dimensional THz images with a step size of $s_{xy} = 10~\mu$m of the structures after the minor loop demagnetization process for the frequencies (a) $f = 1.0$ THz and (b) $f = 1.5$ THz. Two structures, one circle and one rectangle, show domain formation. The other structures switched their magnetization, randomly, as the applied field step resolution was not sufficient to halt the switching at pinning centers.

amplitude. However, two structures exhibit enough pinning centers inside to create domain walls within the applied field parameters. This is shown in Figs. 3(a) and 3(b) in the second row for the circle and the rectangle structure. In these data, the domain walls can be seen as white spaces, with the detected THz e-field amplitude averaged to zero, because within this course resolution, the THz pulse is generated within an area where the magnetization is pointing in

opposite directions. There, the generated THz pulse has two components shifted by $180°$, resulting in a zero signal at the detector. Besides this, the other structures show decreased THz e-field amplitudes, especially on the edges. That hints to a partial domain wall formation, which cannot be resolved in this coarse depiction.

Figure 4 shows the two structures exhibiting magnetic domains scanned in more detail using a smaller step size of $s_{xy} = 2.5~\mu$m. The

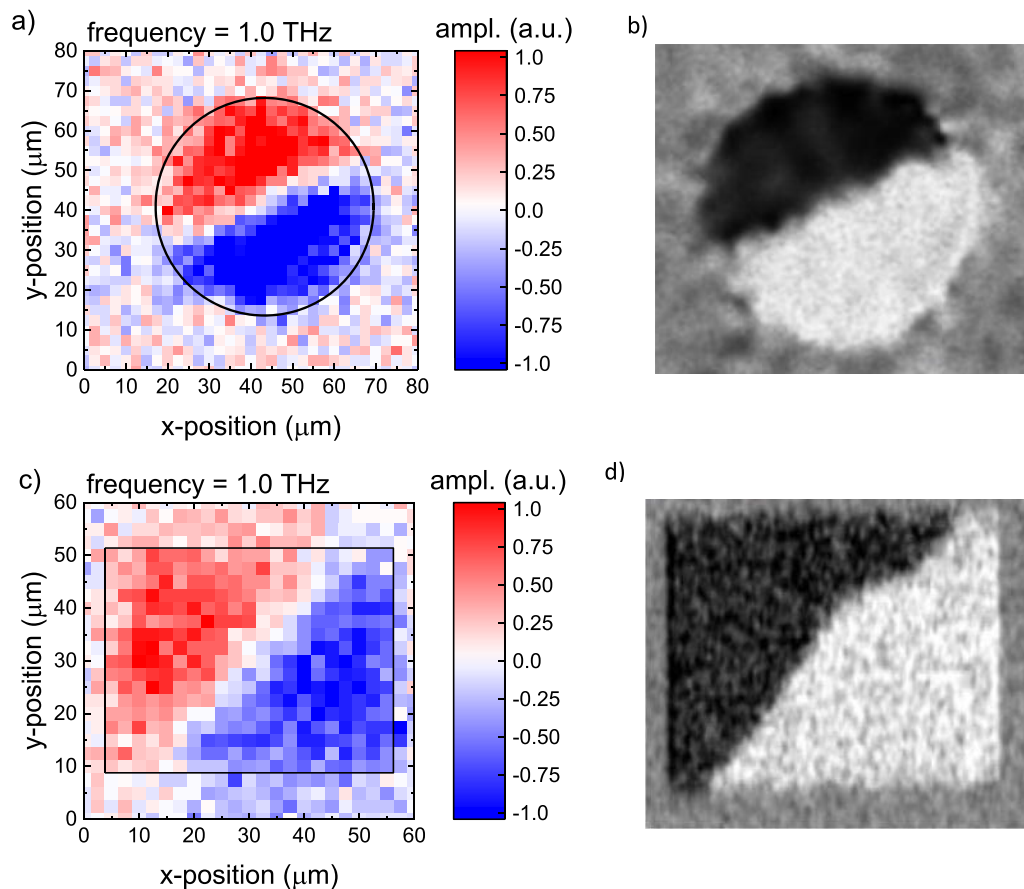**FIG. 4.** Detailed THz imagines of the (a) circle and (c) rectangle after domain wall formation extracted for $f = 1.0$ THz. For comparison, both structures—the circle and the rectangle— imaged by Kerr microscopy are shown in (b) and (d), respectively.

23 January 2024 08:16:28

2D THz scans of the circle [Fig. 4(a)] and the rectangle [Fig. 4(c)] show bisection of the geometric shapes by a domain wall (white). The detected THz signal adds up to zero in the domain wall region because of the magnetization rotation in this area. The structures are divided into a positive (red) and a negative (blue) domain, with magnetization pointing in opposite directions. The THz e-field amplitude in the domain magnetized in the negative direction is slightly larger than that in the positive direction. In general, the THz e-field amplitudes are smaller for the demagnetized samples due to the smaller magnetization in the remanent state, and, thus, a smaller electron polarization is involved in the process generating the inverse spin-Hall effect. In addition, changing the magnetization back and forth, by applying minor loops, blurs the remaining magnetization in the remanent state, leading to different THz e-field amplitudes arriving at the detector for each magnetization direction. Furthermore, Figs. 4(b) and 4(d) show Kerr images of the corresponding structures shown in Figs. 4(a) and 4(c) to ensure the THz images show oppositely magnetized domains instead of a phase shift arising from the instability of other experimental parameters during the measurement. Those could be, e.g., thermal expansion or instabilities leading to a shift of the laser beam. However, both imaging techniques show the same magnetic alignment.

Figure 5 shows the phase shift in the THz e-field amplitude arising from the magnetization direction for two opposite magnetizations $+\mathbf{M}$ (red) and $-\mathbf{M}$ (blue). The THz e-field peak is detected at the same delay position but with an opposite amplitude sign corresponding to a phase shift of $180°$. The signal is recorded by saturating the magnetic structure with an applied field in both magnetization directions. The corresponding FFT for $+\mathbf{M}$ and $-\mathbf{M}$ is depicted in Fig. 5(b). Both magnitudes of the THz e-field amplitude are approximately the same because the magnetization vector is parallel to the easy plane of the FM thin film. The difference stems from fluctuations during the measurement.

The behavior of the THz-amplitudes in the vicinity of a domain wall is shown in more detail in Fig. 6(a) for the circle structure. The measured THz spectra at seven positions across a domain wall are at

a distance of 15 μm. The data show that at the domain wall center (position 4), the THz e-field amplitude is zero for the whole spectrum. At this position, the laser pulse excites electrons within the domain wall and due to its size in both domains. Therefore, two spin currents with opposite spin polarization are generated, and the resulting THz amplitude adds up to zero. Moving away from the domain wall center by 7.5 μm, toward position 1 and 7, the amplitude increases and reaches its maximum at those positions. This corresponds to full spin polarizations reached when a single magnetization area is involved in the THz generation process. For both magnetization directions shown in red and blue, the THz e-field spectra are phase shifted, as expected for opposite spin polarizations. The data clearly show that magnetization change can be detected and magnetic domains can be allocated, including the domain wall positions.

The results of this study show one application for phase-sensitive THz pulse detection using spintronic THz emitters. The emitters can be deposited and structured directly on a glass substrate and can therefore be implemented easily and in a space-saving manner. This ensures identical conditions for THz generation at each emitter spot and makes it possible to image arbitrary shapes in two-dimension, as long as they are lithographically available. The possibility of generating spin currents in differently magnetized domains simultaneously allows us to emit THz radiation with phase shifted e-field amplitudes. In combination with rotation of the sample, this method can be extended to image the domain wall region and investigate the magnetization state.

Furthermore, magnetic structures with a large shape anisotropy, such as stripes and arrays, can be structured in a $90°$ angle to each other. This would allow emission of THz waves with e-field amplitudes oscillating perpendicularly. The only missing component would be an adjustable temporal delay between both perpendicular waves to create phase-controlled THz radiation such as when using a retardation plate. This would allow generation of circular polarized THz radiation of any shape. These possibilities make this imaging technique a new versatile tool for magnetic
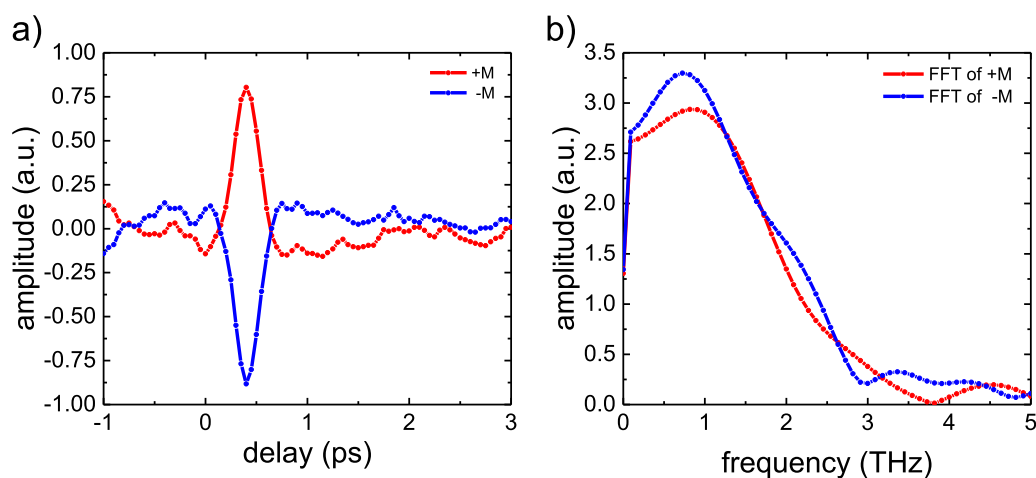
FIG. 5. (a) THz signal recorded in a magnetic field $\mathbf{M}$. Both signals recorded by saturating the magnetization in opposite magnetic fields of 4 mT clearly show a $180°$ phase shift. (b) The Fourier transformed THz frequency amplitudes after zeropadding show a slight difference due to signal fluctuations.
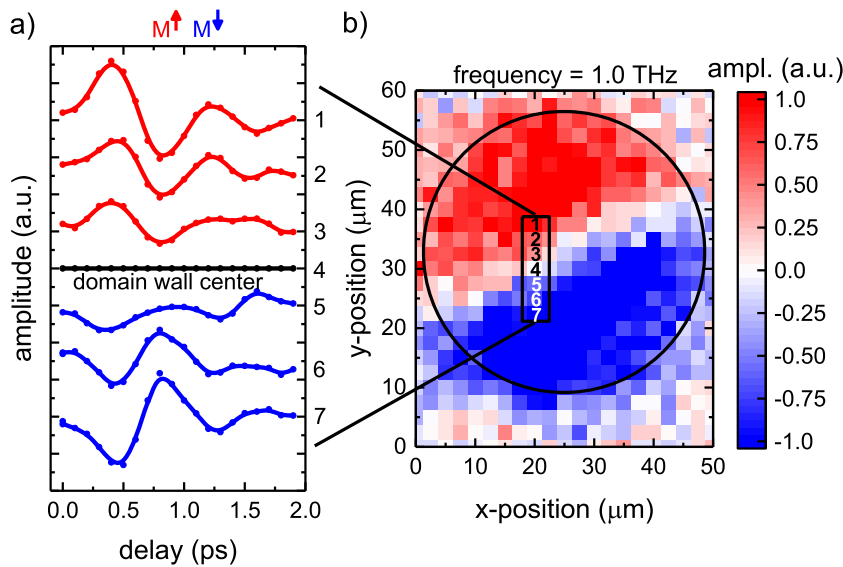
FIG. 6. (a) THz signals at different positions crossing a domain wall. The cross section is 15 μm divided into seven steps with the domain wall center at position 4. The red graphs are magnetized up (positive), and the blue ones are oppositely magnetized down (negative). At (1) and (7), the peak-to-peak value of the THz amplitude reaches its maximum because there, the magnetization is homogeneous in one direction. At a smaller distance from the domain wall, the THz e-field amplitude decreases, with changing magnetization. The extracted THz amplitudes for f = 1.0 THz are marked in the THz image (b).

spectro-microscopy in the THz region with high spatial resolution, imaging magnetization of very small areas fast and without affecting the alignment. A further potential is in the imaging of magnetic insulators, which could be attached in close vicinity to the emitter, using the generated THz radiation to determine their magnetization state in transmission.

In the future, it will be possible to study the magnetization of different shapes depending on their thickness and their influence on the THz radiation. Implementing special collimation lenses will enable examination of even smaller areas and improve the spatial resolution. In addition, by changing the detector to a polarization-independent THz detector, a more detailed representation of the domain walls and the areas in which the rotation of the magnetization takes place will be realized. The useable frequency range can be extended by implementing new techniques for detecting THz radiation, for example, newer generations of PCA or electro-optical detectors such as ZnTe crystals. This makes it possible to study the influence of magnetization in the full frequency range, including higher frequencies (>3 THz).

AUTHOR DECLARATIONS

Conflict of Interest

The authors have no conflicts of interest to disclose.

Author Contributions

Finn-Frederik Stiewe: Formal analysis (lead); Investigation (equal); Validation (equal); Visualization (lead); Writing – original draft (lead); Writing – review & editing (equal). **Tristan Winkel**: Data curation (equal); Formal analysis (equal); Investigation (equal); Software (equal). **Tobias Kleinke**: Investigation (equal); Visualization (equal). **Tobias Tubandt**: Investigation (equal). **Hauke Heyen**: Investigation (equal). **Lucas Vollroth**: Investigation (equal). **Ulrike Martens**: Investigation (equal); Writing – original draft (equal). **Cai Müller**: Data curation (equal); Visualization (equal). **Jeffrey McCord**: Resources (equal); Supervision (equal). **Jakob Walowski**: Project administration (lead); Supervision (lead); Validation (equal); Visualization (equal); Writing – original draft (equal); Writing – review & editing (lead). **Markus Münzenberg**: Funding acquisition (equal); Supervision (equal).

DATA AVAILABILITY

The data that support the findings of this study are available from the corresponding author upon reasonable request.

REFERENCES

[1] S. Parkin and S.-H. Yang, Nat. Nanotechnol. **10**, 195 (2015).

[2] S. S. P. Parkin, M. Hayashi, and L. Thomas, Science **320**, 190 (2008).

[3] R. Wood, J. Magn. Magn. Mater. **321**, 555 (2009).

[4] J. Dubowik, Phys. Rev. B **54**, 1088 (1996).

[5] M. Grimsditch, Y. Jaccard, and I. K. Schuller, Phys. Rev. B **58**, 11539 (1998).

[6] T. Eggebrecht, *Lichtinduzierte Magnetische Defekte in Ultradünnen Filmen* (University in Göttingen, 2018).

[7] T. Eggebrecht, M. Möller, J. G. Gatzmann, N. Rubiano da Silva, A. Feist, U. Martens, H. Ulrichs, M. Münzenberg, C. Ropers, and S. Schäfer, Phys. Rev. Lett. **118**, 97203 (2017).

[8] E. Beaurepaire, J.-C. Merle, A. Daunois, and J.-Y. Bigot, Phys. Rev. Lett. **76**, 4250 (1996).

[9] A. Scholl, L. Baumgarten, R. Jacquemin, and W. Eberhardt, Phys. Rev. Lett. **79**, 5146 (1997).

[10] R. Zhou, Z. Jin, G. Li, G. Ma, Z. Cheng, and X. Wang, Appl. Phys. Lett. **100**, 061102 (2012).

[11] A. V. Kimel, A. Kirilyuk, A. Tsvetkov, R. V. Pisarev, and T. Rasing, Nature **429**, 850 (2004).

[12] C. D. Stanciu, F. Hansteen, A. V. Kimel, A. Kirilyuk, A. Tsukamoto, A. Itoh, and T. Rasing, Phys. Rev. Lett. **99**, 047601 (2007).

[13] T. J. Yen, W. J. Padilla, N. Fang, D. C. Vier, D. R. Smith, J. B. Pendry, D. N. Basov, and X. Zhang, Science **303**, 1494 (2004).

[14] M. Battiato, K. Carva, and P. M. Oppeneer, Phys. Rev. Lett. **105**, 27203 (2010).

[15] T. Seifert, U. Martens, S. Günther, M. A. W. Schoen, F. Radu, X. Z. Chen, I. Lucas, R. Ramos, M. H. Aguirre, P. A. Algarabel, A. Anadón, H. S. Körner, J. Walowski, C. Back, M. R. Ibarra, L. Morellón, E. Saitoh, M. Wolf, C. Song, K. Uchida, M. Münzenberg, I. Radu, and T. Kampfrath, SPIN **07**, 1740010 (2017).

[16] J. Walowski and M. Münzenberg, J. Appl. Phys. **120**, 140901 (2016).

[17] T. S. Seifert, L. Cheng, Z. Wei, T. Kampfrath, and J. Qi, Appl. Phys. Lett. **120**, 180401 (2022).

[18] F.-F. Stiewe, T. Winkel, Y. Sasaki, T. Tubandt, T. Kleinke, C. Denker, U. Martens, N. Meyer, T. S. Parvini, S. Mizukami, J. Walowski, and M. Münzenberg, Appl. Phys. Lett. **120**, 032406 (2022).

[19] E. T. Papaioannou and R. Beigang, Nanophotonics **10**, 1243 (2021).

[20] P. Klarskov, H. Kim, V. L. Colvin, and D. M. Mittleman, ACS Photonics **4**, 2676 (2017).

[21] P. Li, S. Liu, Z. Liu, M. Li, H. Xu, Y. Xu, H. Zeng, and X. Wu, Appl. Phys. Lett. **120**, 201102 (2022).

[22] D. S. Bulgarevich, Y. Akamine, M. Talara, V. Mag-usara, H. Kitahara, H. Kato, M. Shiihara, M. Tani, and M. Watanabe, Sci. Rep. **10**, 1158 (2020).

[23] E. Saitoh, M. Ueda, H. Miyajima, and G. Tatara, Appl. Phys. Lett. **88**, 182509 (2006).

[24] T. Seifert, S. Jaiswal, U. Martens, J. Hannegan, L. Braun, P. Maldonado, F. Freimuth, A. Kronenberg, J. Henrizi, I. Radu, E. Beaurepaire, Y. Mokrousov, P. M. Oppeneer, M. Jourdan, G. Jakob, D. Turchinovich, L. M. Hayden, M. Wolf, M. Münzenberg, M. Kläui, and T. Kampfrath, Nat. Photonics **10**, 483 (2016).

23 January 2024 08:16:28